Appl. Chem. Eng., Vol. 26, No. 3, June 2015, 319-325
http://dx.doi.org/10.14478/ace.2015.1028

Article

분무열분해법으로 CeO_2:Er/Yb 형광체 제조 및 발광특성 최적화

정경열† · 박재훈 · 송신애*

공주대학교 화학공학부, *한국생산기술연구원 마이크로제조시스템기술센터
(2015년 3월 6일 접수, 2015년 4월 9일 심사, 2015년 4월 10일 채택)

Preparation and Luminescence Optimization of CeO_2:Er/Yb Phosphor Prepared by Spray Pyrolysis

Kyeong Youl Jung†, Jea Hoon Park, and Shin Ae Song*

Department of Chemical Engineering, Kongju National University, 1223-24 Cheonan-Daero, Seobuk-gu, Cheonan, Republic of Korea
**Energy Materials Research Center, Korea Research Institute of Chemical Technology, Sinseongno 19, P.O.Box 107, Daejeon 305-600, Republic of Korea*
(Received March 6, 2015; Revised April 9, 2015; Accepted April 10, 2015)

초 록

분무열분해법을 이용하여 서브 미크론 크기의 $CeO_2:Er^{3+}/Yb^{3+}$ 상향 변환 형광체 입자를 합성하고 Er^{3+} 및 Yb^{3+} 농도 변화에 따른 발광특성을 조사하였다. 합성한 $CeO_2:Er^{3+}/Yb^{3+}$는 Er^{3+} 활성이온의 $^4S_{3/2}/^2H_{11/2} \rightarrow {}^4I_{15/2}$ 및 $^4F_{9/2} \rightarrow {}^4I_{15/2}$ 전이에 기인한 강한 녹색 및 적색 발광을 보였다. 가장 높은 발광을 보이는 활성제 농도는 Er = 1.0% 그리고 Yb = 2.0%이며, 농도소광 현상은 쌍극자-쌍극자 상호작용을 통해 일어남이 확인되었다. 레이저 다이오드 여기 광 세기에 대한 발광강도 의존성을 활성이온 농도에 따라 조사하였고, 발광 중간 에너지 레벨의 주 소멸과정을 고려하여 발광 메커니즘을 조사하였다. Yb^{3+}에서 Er^{3+}으로 에너지 전달은 바닥 상태 흡수(ground state absorption, GSA)에 기여하고, Yb^{3+} 도핑은 $^4I_{11/2} \rightarrow {}^4I_{13/2}$ 전이를 가속화시켜 적색/녹색 발광세기 비를 상승시킨다. 최종적으로 분무열분해법으로 제조된 $CeO_2:Er^{3+}/Yb^{3+}$ 형광체의 발광은 선형 감쇠가 중간 에너지 레벨의 고갈을 지배하는 2 광자 프로세스에 의해 일어남을 확인하였다.

Abstract

Submicron-sized $CeO_2:Er^{3+}/Yb^{3+}$ upconversion phosphor particles were synthesized by spray pyrolysis, and their luminescent properties were characterized by changing the concentration of Er^{3+} and Yb^{3+}. $CeO_2:Er^{3+}/Yb^{3+}$ showed an intense green and red emission due to the $^4S_{3/2}$ or $^2H_{11/2} \rightarrow {}^4I_{15/2}$ and $^4F_{9/2} \rightarrow {}^4I_{15/2}$ transition of Er^{3+} ions, respectively. In terms of the emission intensity, the optimal concentrations of Er and Yb were 1.0 % and 2.0%, respectively, and the concentration quenching was found to occur via the dipole-dipole interaction. Upconversion mechanism was discussed by using the dependency of emission intensities on pumping powers and considering the dominant depletion processes of intermediate energy levels for the red and green emission with changing the Er^{3+} concentration. An energy transfer from Yb^{3+} to Er^{3+} in CeO_2 host was mainly involved in ground-state absorption (GSA), and non-radiative relaxation from $^4I_{11/2}$ to $^4I_{13/2}$ of Er^{3+} was accelerated by the Yb^{3+} co-doping. As a result, the Yb^{3+} co-doping led to greatly enhance the upconversion intensity with increasing ratios of the red to green emission. Finally, it is revealed that the upconversion emission is achieved by two photon processes in which the linear decay dominates the depletion of intermediate energy levels for green and red emissions for $CeO_2:Er^{3+}/Yb^{3+}$ phosphor.

Keywords: *Upconversion phosphor, Spray pyrolysis, Energy transfer, two-photon process*

1. Introduction

Upconversion (UC) materials converting near-infrared (NIR) into visible light have drawn great attention in many research areas such as bio-imaging, security ink, 3D displays, and solar cells[1-5]. Host materials for UC phosphors should have low phonon energy to achieve efficient emission. The emission wavelength and upconversion intensity are influenced by host compositions even though the same activators are used. A number of materials including fluorides, chlorides, sulfides and oxides have been considered as the UC host[6-9]. Among these, most of researches have been performed on fluorides (e.g. $NaYF_4$) due to their low phonon energy[10-14]. Fluorides not only have weak chemical and thermal stability, but also can deliquesce with generating

† Corresponding Author: Kongju National University, Department of Chemical Engineering, 1223-24 Cheonan-Daero, Seobuk-gu, Cheonan, Republic of Korea
Tel: +82-41-554-2640 e-mail: kyjung@kongju.ac.kr

pISSN: 1225-0112 eISSN: 2288-4505

HF which causes a safety problem in a preparation procedure, which may be obstacle to their practical application[15]. On the contrary, oxide-based UC phosphors have good chemical and thermal properties. Thus, recently, the development of oxide-based UC phosphors with good optical properties has received great attention for various practical applications.

Suitable selection of oxide matrix is critical to obtain the high emission efficiency for oxide-based UC phosphors. A number of simple oxides, such as Y_2O_3, Gd_2O_3, ZrO_2, Lu_2O_3 and La_2O_3, have been investigated as a host for UC phosphors due to their low vibrational frequencies[16-22]. Recently, CeO_2 was reported as a promising host for UC phosphor because it has low phonon cutoff energy and excellent thermal stability[23-25]. In addition, it has the same crystal structure as erbium and ytterbium, which facilitates the substitution of activators into the CeO_2 host lattices.

To achieve high luminescence, activators and sensitizers should be well distributed into ceria lattices without any phase segregation. Thus, it is important to select a proper synthetic method in terms of preparing high upconversion phosphors. Spray pyrolysis is one of excellent synthetic processes and has been used to prepare multi-component functional materials like phosphor[26-29]. Since one droplet containing precursors is turned to one particle in the spray pyrolysis, all ingredients in one particle is able to be mixed well at the nanoscale. Nevertheless, to our best knowledge, there are no reports on the synthesis of CeO_2-based upconversion phosphors via the spray pyrolysis. In this work, $CeO_2:Er^{3+}/Yb^{3+}$ upconversion phosphor particles were synthesized by spray pyrolysis. The concentrations of Er^{3+} and Yb^{3+} were optimized in terms of the luminescence intensity of $CeO_2:Er^{3+}/Yb^{3+}$. The luminescent quenching property and the upconversion mechanism were studied by changing the concentration of Er^{3+} and Yb^{3+}.

2. Experimental

$Ce_{1-x-y}O_2:Er^{3+}_x,Yb^{3+}_y$ upconversion phosphor particles were prepared by a spray pyrolysis process which consists of an ultrasonic aerosol generator with 17 vibrators of 1.7 MHz, a quartz tube (inner diameter = 55 mm, length = 1000 mm), and a Teflon bag filter. Cerium nitrate (Aldrich, 99%), erbium oxide (Aldrich, 99.99%), and ytterbium oxide (Alfa, 99.99%) were used as the precursor of Ce, Er, and Yb, respectively. 1.0 wt% Er_2O_3 aqueous solution was prepared according to the following procedure. 1g Er_2O_3 was first dissolved in nitric acid solution, and followed by adding purified water until the solution weight reaches 100 g. As the same manner, 1.0 wt% solution of Yb_2O_3 was prepared in advance. The exact quantities of activators required when varying the Er or Yb concentration in the $Ce_{1-x-y}O_2:Er^{3+}_x,Yb^{3+}_y$ phosphor particles was measured by taking the weight of the two activator aqueous solutions prepared in advance. The spray solutions were prepared by dissolving cerium nitrate in the aqueous solution containing each activator. The total concentration of the precursors was fixed at 0.2 M. The Er^{3+} (x) concentrations were varied from 0.005 to 0.06, and the Yb concentrations (y) were controlled from 0.01 to 0.07. The

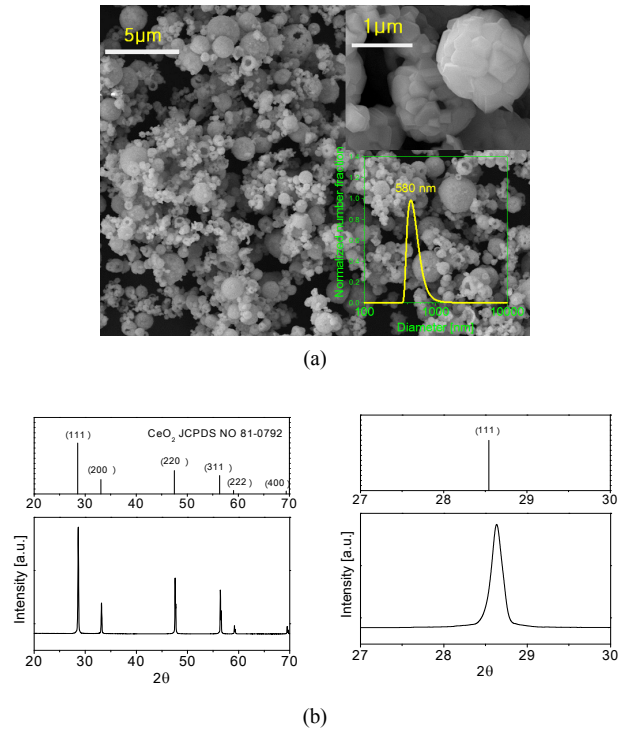

Figure 1. (a) SEM photo (inset-particle size distribution) and (b) XRD pattern of CeO_2:Er/Yb particles prepared by spray pyrolysis.

spray solutions were atomized to droplets which were carried by air (30 liter/min) into the quartz tube reactor at 900 ℃. The powders were collected by the Teflon bag filter installed at the end of the quartz reactor. The obtained precursor powders were followed by a thermal treatment at 1300 ℃ for 3 h in a box furnace under an air environment.

The emission properties of the prepared phosphor particles were investigated by using a fluorescence spectrometer (Perkin Elmer, LS 55) under the excitation of 975 nm light pumped by an IR Laser (Optoenergy, PL980P330J). Changes in the emission intensity were monitored by varying the power of the IR source from 100 to 1000 mW. The crystal structure was identified by X-ray diffraction (XRD, Rigaku, D/Max-RB) using Cu K_a radiation (λ = 1.5418 Å). The morphology of the prepared phosphor particles were monitored by using scanning electron microscopy (SEM, TESCAN, MIRA LMH). Particle size distribution was measured by using a particle size analyzer (DLS, Photal Otsuka Electronics).

3. Results and discussion

Figure 1(a) shows the morphology and size distribution of phosphor particles prepared by spray pyrolysis. The particles have spherical shape, but hollow structure. The average particle size is about 580 nm. The hollow structure indicates that the precipitation of the precursor salts begins at the surface of droplets because the surface concentration of salts first reaches the supercritical saturation due to the fast drying of water. According to the SEM result, no particle agglomeration oc

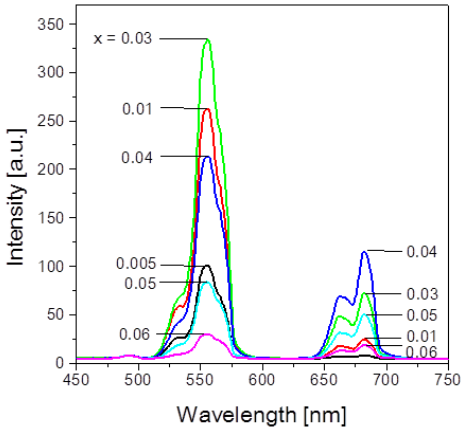

(a)

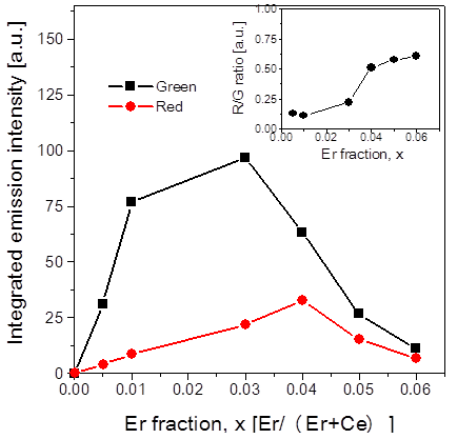

(b)

Figure 2. (a) Upconversion emission spectra of $Ce_{1-x}O_2$:Erx particles and (b) the emission intensity (inset-the emission ratio of red to green) as a function of Er content.

curs during the post thermal treatment at 1300 °C. To achieve high luminescence, phosphors should have high crystallinity and activators should be inserted in host lattice sites. According to the XRD analysis as shown in Figure 1(b), the prepared particles have the cubic fluorite-type CeO_2 structure (JCPDS No. 81-0792) without any phase formation for Er_2O_3 and Yb_2O_3 crystalline. The peak for (111) phase shifts toward a large diffraction angle compared with pure cerium oxide, indicating that the rare-earth activators are successfully doped into the host lattice.

Figure 2(a) shows the upconversion spectra of $Ce_{1-x}O_2:Er_x$ particles prepared by changing the Er concentration. The integrated intensity for green and red emission is shown in Figure 2(b) as a function of the Er concentration. In the green region, the peaks at 537 nm and 556 nm are due to the $^2H_{11/2} \rightarrow {}^4I_{15/2}$ and $^4S_{3/2} \rightarrow {}^4I_{15/2}$ transitions of Er ions, respectively. The red emission in the wavelength range of 650~700 nm is attributed to the $^4F_{9/2} \rightarrow {}^4I_{15/2}$ transition. As increasing the Er content, the intensity for the green and red emission increases and reaches to the maximum value at x = 0.03 and x = 0.04, respectively. This means that both of the $^4S_{3/2} \rightarrow {}^4I_{15/2}$ and the $^4F_{9/2} \rightarrow {}^4I_{15/2}$ transitions are accelerated simultaneously by increasing the Er concentration up to 3% (x = 0.03). When the Er concentration is larger than 3%, there is the concentration quenching which lowers the entire emission intensity. The inset of Figure 2(b) shows the dependence of the R/G ratio (red emission/green emission) on the Er concentration. When the Er content is 3% and larger, the R/G ratio increases, indicating that the non-radiative decay from the $^4S_{3/2}$ level to the red-emitting level ($^4F_{9/2}$) is populated by increasing the Er concentration.

Figure 3(a) and (b) show the Yb^{3+} co-doping effect on the emission properties. The Yb^{3+} doping clearly enhances both green and red emission due to the resonant energy transfer (ET) from Yb^{3+} to Er^{3+}[24-25]. The green emission intensity is strongest at y = 0.02 (2% with respect to Ce), whereas for the red emission the concentration quenching begins at y = 0.03 (3%). However, the green emission dramatically decreases when the Yb^{3+} content is 3% and larger. As shown in the inset of Figure 3(b), the ratio of red to green in the emission intensity increases monotonically with increasing the Yb^{3+} concentration. These results indicate that the Yb^{3+} doping evidently enhances the absorption of the IR photons, and that the ET processes involved in the red emission are accelerated by increasing the Yb^{3+} concentration. In terms of optimizing the emission intensity of $CeO_2:Er^{3+},Yb^{3+}$ phosphor at y = 0.02, the fine tuning in the Er^{3+} concentration was carried out and the results were shown in Figure 3(c) and (d). The highest intensity was observed at x = 0.01 and 0.015 for the green and red emission, respectively. As shown in Figure 3(d), the R/G ratio was also enlarged linearly as increasing the Er^{3+} content. This is consistent with the result for the Er concentration effect when no Yb^{3+} is co-doped as shown in Figure 2. On the basis of all results obtained from the variation of Er and Yb concentrations, the optimal composition in terms of the total emission intensity was determined as $(Ce_{0.97}, Er_{0.01}, Yb_{0.02})O_2$.

For phosphor materials, a concentration quenching in the emission intensity occurs due to the non-radiative decay of excited photons to the ground state of activators. On the basis of the concentration quenching observed, the critical distance (R_c) for the non-radiative energy transfer can be calculated by the following equation[30].

$$R_c \approx 2\left(\frac{3V}{4\pi x_c N}\right)^{1/3} \quad (1)$$

where x_c is critical concentration, V is the unit cell volume (158.5 Å), and N is the number of Z ions (N = 4). As shown in Figure 2 and Figure 3, the concentration quenching was observed when the activator concentration (Er or Er/Yb) was 0.03. Then, the calculated critical distance is 14 Å. The non-radiative energy transfer occurs mainly due to an exchange interaction or an electric multipolar interaction between activators. In general, the non-radiative energy transfer of forbidden transition occurs via the exchange interaction, typically with the critical distance of about 5 Å[31]. Thus, the energy transfer for $CeO_2:Er^{3+},Yb^{3+}$ phosphor should be controlled by an electric multipolar interaction process.

The relation between the emission intensity (I) and the activator

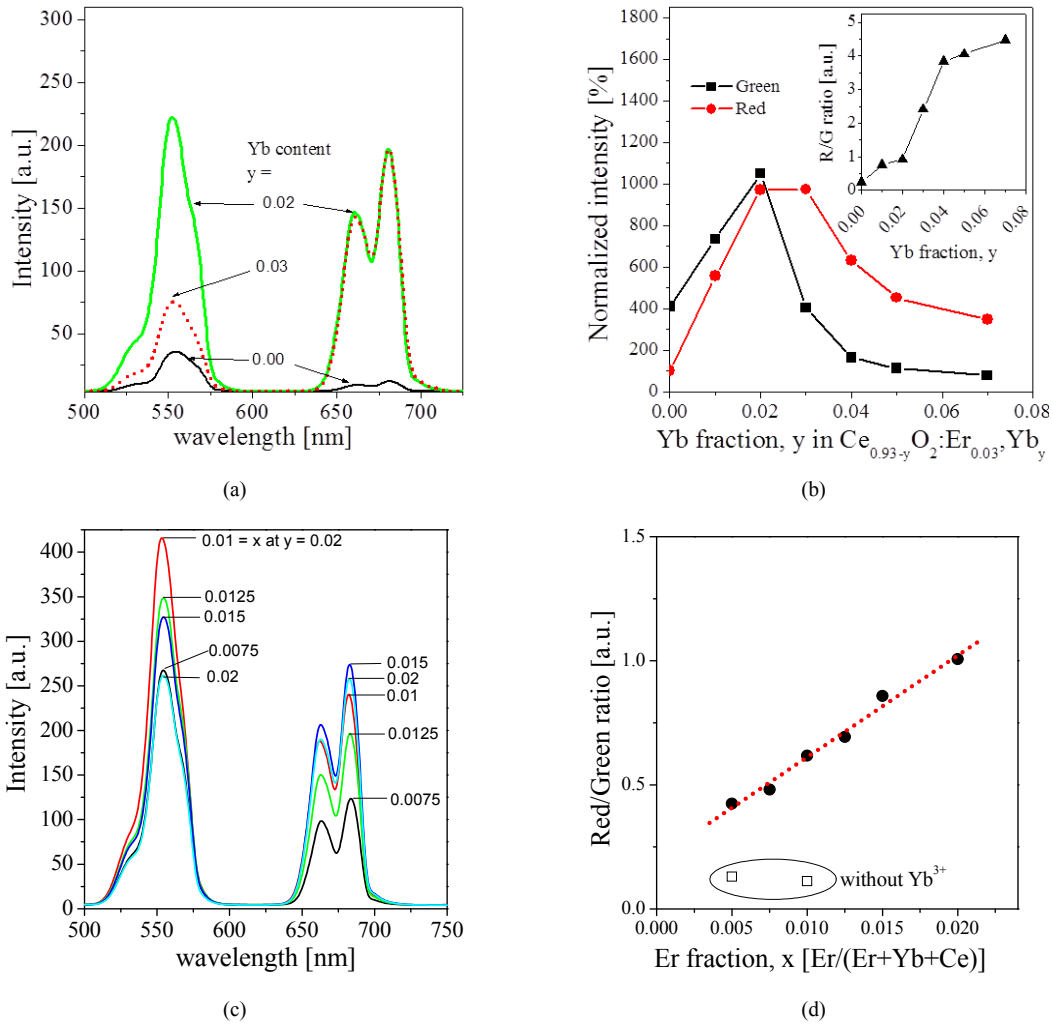

Figure 3. (a) Upconversion emission spectra and (b) the emission intensity (normalized by the intensity of red emission for $Ce_{0.97}O_2:Er^{3+}_{0.03}$) as a function of Yb^{3+} content for $Ce_{0.97-y}O_2:Er^{3+}_{0.03},Yb^{3+}_{y}$. (c) Emission spectra and (d) red/green ratio with changing the Er concentration for $Ce_{0.98-x}O_2:Er^{3+}_{x},Yb^{3+}_{0.02}$.

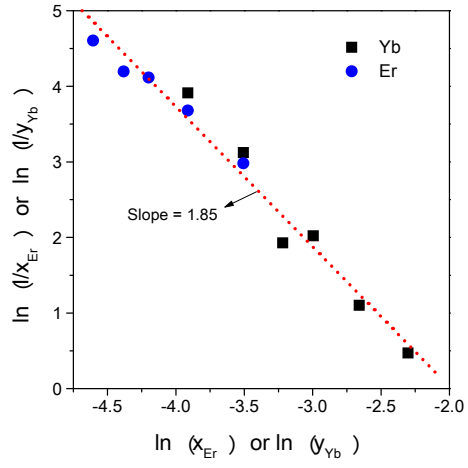

Figure 4. The relationship between ln(*I*/*x* or *I*/*y*) vs. ln(*x* or *y*) for $Ce_{1-x-y}O_2:Er^{3+}_{x},Yb^{3+}_{y}$ phosphor particles prepared by spray pyrolysis.

concentration was used to elucidate the type of multipolar interactions involved in the energy transfer[32].

$$\frac{I}{x}=\frac{K}{1+\beta x^{Q/3}} \tag{2}$$

where K and β are constants for the interaction. Q is the electric multipolar character which has 3, 6, 8, and 10 for the exchange interaction, dipole-dipole, dipole-quadruple, and quadruple-quadruple interactions, respectively. Under the assumption that $\beta x^{Q/3} >> 1$, Eq. (2) can be expressed as follows.

$$\ln\left(\frac{I}{x}\right)=A-\frac{Q}{3}\ln x \ (A=\ln K-\ln \beta) \tag{3}$$

Figure 4 shows the fitting of $\ln(I/x_{Er})$ versus $\ln(x_{Er})$ for $CeO_2:Er^{3+}$ and $\ln(I/C_{Er+Yb})$ versus $\ln(C_{Er+Yb})$ for $CeO_2:Er^{3+}/Yb^{3+}$. The calculated

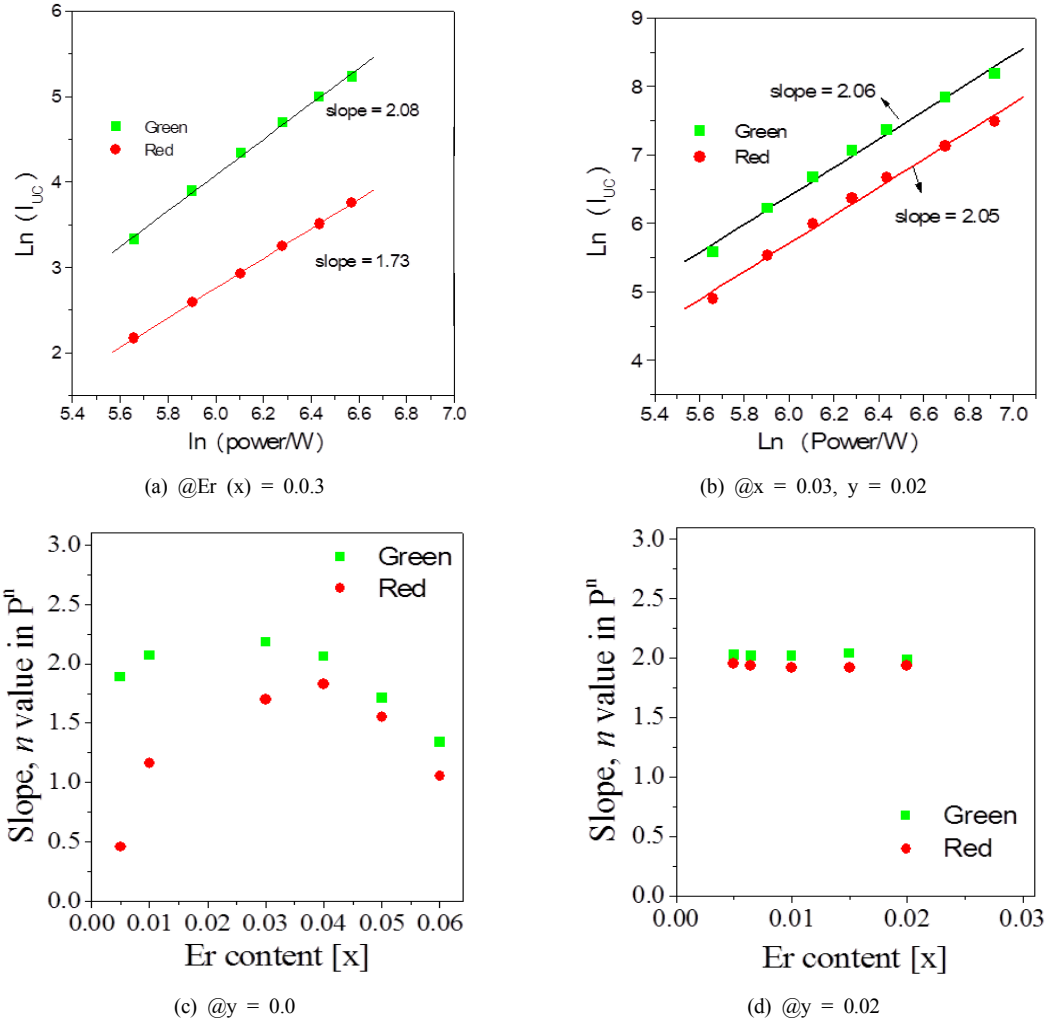

Figure 5. Logarithmic dependence of upconversion emission intensity with respect to IR imput power (a) CeO_2:Er and (b) CeO_2:Er,Yb phosphors. (c) and (d) are *n* values in the $I_{UC} \propto P^n$ relation as a function of Er or Yb content.

slopes are -2.30 and -2.26 for $CeO_2:Er^{3+}$ and $CeO_2:Er^{3+}/Yb^{3+}$, respectively. That is, the Q value can be considered to be close to 6. From this calculation, the luminescence quenching in $CeO_2:Er^{3+}$ or $CeO_2:Er^{3+}/Yb^{3+}$ was confirmed to occur mainly via the dipole-dipole interaction.

To more understand the upconversion mechanism in $CeO_2:Er^{3+}/Yb^{3+}$, the emission intensity (I_{UC}) under the 975 nm irradiation was recorded as a function of laser-pumping power (P). The emission intensity has the $I_{UC} \propto P^n$ relation where n is the number of absorbed pump photons. Figure 5(a) and (b) show the ln(I_{UC}) versus ln(P) plots for the phosphor composition of $(Ce_{0.97}, Er_{0.03})O_2$ and $(Ce_{0.97}, Er_{0.03}, Yb_{0.02})O_2$. Then, n can be obtained from the slope. The n value should be close to 2 for two photon processes. The resulted slopes of $CeO_2:Er^{3+}$ were 2.08 for green and 1.73 for red. Whereas, the slopes for the green and red emission for $CeO_2:Er^{3+}/Yb^{3+}$ were 2.06 and 2.05, respectively. Based on a simplified three-level system for Er^{3+}/Yb^{3+} co-doping phosphor, Lei et al. examined in detail the upconversion mechanism regarding the competition between linear decay and upconversion processes[33]. According to the suggested mechanism, the up-conversion intensity (I_{UC}) is proportional to P^2 when the linear decay dominates the depletion of photons in intermediate states. Inversely, if the up-conversion is dominant, I_{UC} is proportional to P. For green emission, the n values are 2.08 and 2.06 for $(Ce_{0.997}, Er_{0.03})O_2$ and $(Ce_{0.995}, Er_{0.03}, Yb_{0.02})O_2$, respectively. Given this, the green emission is achieved by two-photon processes in which the linear decay is dominant. The red emission has n = 1.73 when no Yb^{3+} is doped, indicating that the depletion of intermediate state is achieved by the competition between linear decay and upconversion.

Figure 5(c) shows the change in n values as a function of Er^{3+} concentrations for $CeO_2:Er^{3+}$ samples. When Er^{3+} contents are lower than a critical concentration (4%), n values for green emission are maintained closely to~2. Therefore, the linear decay is dominant in the depletion of photons in intermediate levels for green emission. On the contrary, n values for red emission are largely changed with changing the Er^{3+} concentration. Given that the n values of red emission decrease with reducing the Er^{3+} concentration, upconversion dominates

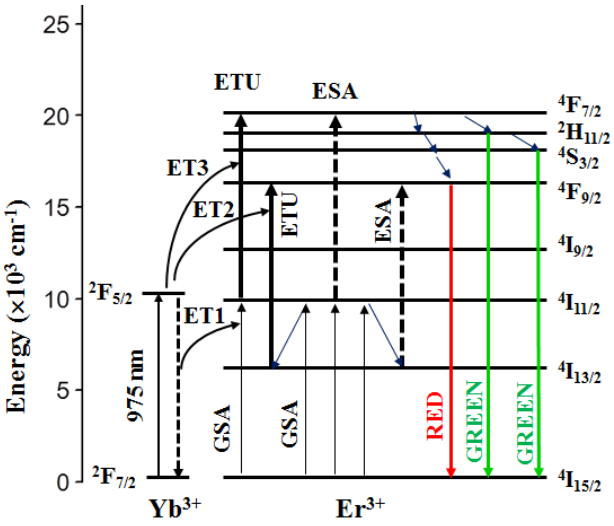

Figure 6. Schematic diagram for the energy levels of the Er^{3+}/Yb^{3+} codoped CeO_2.

depletion of photons in intermediate energy levels at low Er concentrations when no Yb^{3+} is doped. As increasing the Er^{3+} content larger than the critical concentration, the *n* values of both green and red emissions approach to~1.0. Consequently, the upconversion becomes the dominant depletion of photons in the intermediate energy levels.

Figure 5(d) shows the change in n values with changing the Er^{3+} concentration at y = 0.02 (Yb^{3+} = 2.0%). For both green and red emissions, the *n* values are close to 2 and maintained in the Er^{3+} concentration range in which no luminescence quenching is observed. This result indicates that an effective energy transfer from Yb^{3+} to Er^{3+} occurs in upconversion processes. In particular, the major depletion of photons in intermediate energy levels for red emission is changed by the Yb^{3+} doping. The possible energy level diagram of Er^{3+}/Yb^{3+} system in CeO_2 host is shown in Figure 6. There are three paths for the energy transfer (ET) from Yb^{3+} to Er^{3+}, which are indicated as ET1, ET2 and ET3 in Figure 6. If the energy transfer from Yb^{3+} to Er^{3+} mainly occurs in intermediate energy levels (ET2 and ET3), the *n* values for red emission in Figure 5(d) should be smaller than 2.0. However, this situation does not agree with the experimental results. The photon density in the $^4I_{13/2}$ state (intermediate level of red emission) should be increased by the Yb^{3+} co-doping so that the linear decay is a dominant depletion. To achieve this situation, the energy transfer from Yb^{3+} to Er^{3+} is needed to contribute a lot to the GSA process (ET1) of Er^{3+} ions. As a result, the photon density of the $^4I_{11/2}$ energy levels increases largely. Also, a lot of photons excited by the energy transfer should be involved in the $^4I_{11/2} \rightarrow {}^4I_{13/2}$ relaxation, which makes the linear decay to be dominant depletion of intermediate energy levels for green emission. At the same time, the increased photons in the $^4I_{13/2}$ state accelerate the linear decay to the ground state ($^4I_{15/2}$). As a result, the linear decay dominates the depletion of photons in the intermediate level of red emission, and the slope of the red emission with changing the pumping power is turned to be~2 at low Er^{3+} concentrations when Yb^{3+} ions are codoped.

4. Conclusions

Spherical submicron-sized $CeO_2:Er^{3+}/Yb^{3+}$ particles were synthesized by spray pyrolysis. The unpconversion properties were characterized by changing the Er^{3+} and Yb^{3+} concentration. In terms of achieving the highest upconversion emission, the optimal composition was $(Ce_{0.97}, Er_{0.01}, Yb_{0.02})O_2$. The concentration quenching was confirmed to occur via the dipole-dipole interaction. From the dependence of emission intensities on the pumping power, the dominant depletion path of excited photons in intermediate levels was elucidated. For $CeO_2:Er^{3+}$ samples having the Er^{3+} concentrations lower than 4.0%, the linear decay was dominant for green emission, whereas the red emission was achieved by competition between linear decay and upconversion. The Yb^{3+} co-doping clearly enhanced both the green and the red emission as the consequence of the effective resonant energy transfer from Yb^{3+} to Er^{3+} ions. When the Yb^{3+} ions were introduced, the red as well as green emissions were found to be achieved by two-photon processes having the linear decay as the dominant depletion of intermediate energy levels. The energy transfer in $CeO_2:Er^{3+}/Yb^{3+}$ phosphor was mainly involved in the GSA process, which resulted in the increase of photons in the $^4I_{11/2}$ energy and accelerated the non-radiative relaxation from $^4I_{11/2}$ to $^4I_{13/2}$. As a result, the Yb^{3+} co-doping led to increase the ratio of red to green emission, and the dominant depletion of photons in the $^4I_{13/2}$ intermediate levels for red emission was achieved by the linear decay.

References

1. Q. Li, W. Feng, and F. Li, Water-soluble lanthanide upconversion nanophosphors: Synthesis and bioimaging applications *in vivo*, *Coord. Chem. Rev.*, **273-274**, 100-110 (2014).
2. T. R. Hinklin, S. C. Rand, and R. M. Laine, Transparent, Polycrystalline Upconverting Nanoceramics: Towards 3-D Displays, *Adv. Mater.*, **20**, 1270-1273 (2008).
3. J. M. Meruga, A. Baride, W. Cross, J. J. Keller, and P. S. May, Red-green-blue printing using luminescence-upconversion inks, *J. Mater. Chem. C*, **2**, 2221-2227 (2014).
4. E. H. Song, S. Ding, M. Wu, S. Ye, Z. T. Chen, Y. Y. Ma, and Q. Y. Zhang, Tunable white upconversion luminescence from Yb^{3+}-Tm^{3+}-Mn^{2+} tri-doped perovskite nanocrystals, *Opt. Mater. Express*, **4**, 1186-1196 (2014).
5. M. J. Lim, Y. N. Ko, Y. C. Kang, and K. Y. Jung, Enhancement of light-harvesting efficiency of dye-sensitized solar cells via forming TiO_2 composite double layers with dwon/up converting phosphor dispersion, *RSC Adv.*, **4**, 10039-10042 (2014).
6. M. He, P. Huang, C. Zhang, J. Ma, R. He, and D. Cui, Phase- and size-controllable synthesis of hexagonal upconversion rare-earth fluoride nanocrystals through an oleic acid/ionic liquid two-phase system, *Chem. Eur. J.*, **18**, 5954-5969 (2012).
7. M. Ding, D. Chen, T. Chen, C. Lu, Y. Ni, and Z. Xu, Hydrothermal synthesis and upconversion luminescence properties of BaFCl:Yb^{3+}/Er^{3+} microhseets, *Mater. Lett.*, **128**, 101-104 (2014).
8. Y. Song, Y. Huang, L. Zhang, Y. Zheng, N. Guo, and H. You, Gd_2O_2S:Yb,Er submicrospheres with multicolor upconversion fluo-

rescence, *RSC Adv*., **2**, 4777-4781 (2012).
9. F. Vetrone, J.-C. Boyer, J. A. Capobianoco, A. Speghini, and M. Bettinelli, Concentration-dependent near-infrared to visible upconversion in nanoscrystalline and bulk $Y_2O_3:Er^{3+}$, *Chem. Mater.*, **15**, 2737-2743 (2013).
10. J.-H. Zeng, J. Su, Z.-H. Li, R.-X. Yan, and Y.-D. Li, Synthesis and upconversion luminescence of hexagonal-phase $NaYF_4:Yb,Er^{3+}$ phosphors of controlled size and morphology, *Adv. Mater*., **17**, 2119-2123 (2005).
11. C. Mi, Z. Tian, C. Cao, Z. Wang, C. Mao, and S. Xu, Novel microwave-assisted solvothermal synthesis of $NaYF_4$:Yb,Er upconversion nanoparticles and their application in cancer cell imaging, *Langmuir*, **27**, 14632-14637 (2011).
12. J. Zhao, Z. Lu, Y. Yin, C. Mcrae, J. A. Piper, J. M. Dawes, D. Jin, and E. M. Goldys, Upconversion luminescence with tunable lifetime in $NaYF_4$:Yb,Er nanocrystals: role of nanocrystal size, *Nanoscale*, **5**, 944-952 (2013).
13. M. Haase and H. Schäfer, Upconverting nanoparticles, *Angew. Chem. Int. Ed*., **50**, 5808-5829 (2011).
14. X. Liu, X. Zhang, G. Tian, W. Yin, L. Yan, L. Ruan, Z. Yang, D. Xiao, and Z. Gu, A simple and efficient synthesis route for preparation of $NaYF_4$ upconversion nanoparticles by thermo-decomposition of rare-earth oleates, *Cryst. Eng. Comm.*, **16**, 5650-5661 (2014).
15. Q. Xiao, G. Dong, and J. Qiu, Synthesis and up-conversion luminescence of Yb^{3+}/Ln^{3+} (Ln = Er, Tm, Ho) co-doped strontium cerate by Pechini method, *J. Am. Ceram. Soc.*, **97**, 1899-1904 (2014).
16. F. Vetrone, J. C. Boyer, J. A. Capobianco, A. Speghini, and M. Bettinelli, Effect of Yb^{3+} codoping on the upconversion emission in nanocrystalline $Y_2O_3:Er^{3+}$, *J. Phys. Chem. B*, **107**, 1107-1112 (2003).
17. D. Matsuura, H. Hattori, and A. Takano, Upconversion luminescence properties of Y_2O_3 nanocrystals doped with trivalent rare-earth ions, *J. Electrochem. Soc*., **152**, H39-H42 (2005).
18. Y. Dwivedi, A. Bahadur, and S. B. Rai, Optical avalanche in Ho:Yb:Gd_2O_3 nanocrystals, *J. Appl. Phys*., **110**, 043103-043103 (2011).
19. V. Singh, V. K. Rai, K. Al-Shamery, M. Haase, and S. H. Kim, NIR to visible frequency upconversion in Er^{3+} and Yb^{3+} codoped ZrO_2 phosphor, *Appl. Phys. A*, **113**, 747-753 (2013).
20. K. Zheng, W. Song, C. Lv, Z. Liu, and W. Qin, Controllable synthesis and size-dependent upconversion luminescence properties of $Lu_2O_3:Yb^{3+}/Er^{3+}$ nanospheres, *Cryst. Eng. Comm.*, **16**, 4329-4337 (2014).
21. J. Yang and J. Lin, Sol-gel synthesis of nanocrystalline Yb^{3+}/Ho^{3+}-doped Lu_2O_3 as an efficient green phosphor, *J. Electrochem. Soc*., **157**, K273-K278 (2010).
22. Z. Xu, Q. Zhao, Y. Sun, B. Ren, L. You, S. Wang, and F. Ding, Synthesis of hollow $La_2O_3:Yb^{3+}/Er^{3+}$ microspheres with tunable up-conversion luminescence properties, *RSC Adv*., **3**, 8407-8416 (2013).
23. X. Liu, S. Chen, and X. Wang, Synthesis and photoluminescence of $CeO_2:Eu^{3+}$ phosphor powder, *J. Lumin*., **127**, 650-654 (2007).
24. J.-H. Cho, M. Bass, S. Babu, J. M. Dowding, W. T. Self, and S. Seal, Up conversion luminescence of Yb_{3+}-Er_{3+} codoped CeO_2 nanocrystals with imaging applications, *J. Lumin*., **132**, 743-749 (2012).
25. Z. Wang, F. Gu, Z. Wang, and D. Han, Solvothermal synthesis of CeO_2:Er/Yb nanorods and upconversion luminescence characterization, *Mater. Res. Bull.*, **53**, 141-144 (2014).
26. K. Y. Jung, H. W. Lee, Y. C. Kang, S. B. Park, and Y. S. Yang, Luminescent properties of (Ba,Sr)$MgAl_{10}O_{17}$:Mn,Eu green phosphor prepared by spray pyrolysis under VUV excitation, *Chem. Mater*., **17**, 2729-2734 (2005).
27. M. C. Maniquiz, K. Y. Jung, and S. M. Jeong, Luminescence Characteristics of $Y_3Al_{5-2y}(Mg,Si)_yO_{12}$:Ce phosphor prepared by spray pyrolysis*, J. Electrochem. Soc*., **157**, H1135-H1139 (2010).
28. J. H. Kim and K. Y. Jung, Luminescence characteristics and optimization of (La,Gd)Sr_2(A,B)O_5:Ce phosphor for white light emitting diodes, *J. Lumin*., **132**, 1376-1381 (2012).
29. W. Chung, H. J. Yu, S. H. Park, B.-H. Chun, J. Kim, and S. H. Kim, Spray pyrolysis synthesis of $MAl_2O_4:Eu^{2+}$ (M=Ba, Sr) phosphor for UV LED excitation, *J. Cryst. Growth*, **326**, 73-76 (2011).
30. J. H. Kim and K. Y. Jung, Preparation and luminescence characterization of fine-sized $LaSr_2AlO_5$:Ce phosphor prepared by spray pyrolysis, *J. Lumin.*, **131**, 1487-1491 (2011).
31. D. L. Dexter, A theory of sensitized luminescence in solids, *J. Chem. Phys*., **31**, 836-850 (1953).
32. S. H. M. Poort, W. P. Blocpoel, and G. Blasse, Luminescence of Eu^{2+} in barium and strontium aluminate and gallate, *Chem. Mater*., **7**, 1547-1551 (1995).
33. Y. Lei, H. Song, L. Yang, L. Yu, Z. Liu, G. Pan, X. Bai, and L. Fan, Upconversion luminescence, intensity saturation effect, and thermal effect in $Gd_2O_3:Er^{3+},Yb^{3+}$ nanowire, *J. Chem. Phys*., **123**, 174710 (2005).